Supporting Information for

Surface acidity and As(V) complexation of iron oxyhydroxides: insights from first principles molecular dynamics simulations

Yingchun Zhang,[†] Xiandong Liu,[*,†] Jun Cheng,[‡] Xiancai Lu[†]

[†]State Key Laboratory for Mineral Deposits Research, School of Earth Sciences and Engineering, Nanjing University, Nanjing, Jiangsu 210023, P. R. China

[‡]College of Chemistry and Chemical Engineering, Xiamen University, Xiamen, Fujian 361005, P. R. China

*Corresponding author: xiandongliu@nju.edu.cn. Tel: +86 25 83594664, Fax: +86 25 83686016.

Number of pages: 22

Number of tables: 5

Number of figures: 12

This file includes the following contents:

S1. Density profiles of water

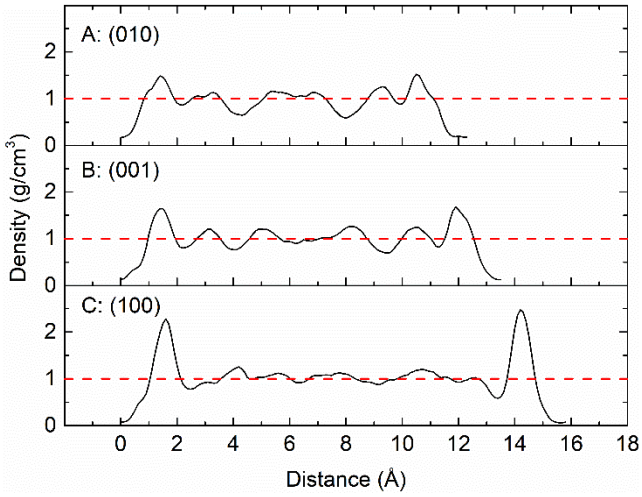

Figure S1. Water density profiles of (A) (010), (B) (001), and (C) (010) systems. The mid-plane between surface O atoms and first-layer water O atoms was taken as the starting point of the density profile for each system. It is clear that the densities in the middle regions are very close to 1.00 g/cm^3 and the density distributions are approximately symmetric with respect to the center of the solution regions.

S2. pK$_a$ calculation method

Table S1. Fe-Fe and Fe-O distances (in Å) in the central layers of the slabs and bulk crystal. $d1_{\text{Fe-Fe}}$ is the distance between iron atoms in the same iron layer; $d2_{\text{Fe-Fe}}$ is the distance between iron atoms in different iron layers of the same lepidocrocite sheet; $d_{\text{Fe-O}}$ is the distance between iron and oxygen atom of hydroxyl group.

Systems	$d1_{\text{Fe-Fe}}$	$d2_{\text{Fe-Fe}}$	$d_{\text{Fe-O}}$
bulk	3.06	3.08	2.01
(010)	3.06	3.06	2.00
(001)	3.06	3.06	2.01
(100)	3.05	3.08	2.01

The pK_a values of lepidocrocite surface groups were evaluated via the half-reaction scheme of the vertical energy gap method.[1, 2] With this scheme, the proton of the acid site (labeled as AH) is gradually transformed into a classical particle with no charge (i.e. the dummy atom). The free energy change associated with this process is calculated with the thermodynamic integration relation:

$$\Delta_{dp}A_{AH} = \int_0^1 d\eta \left\langle \Delta_{dp}E_{AH} \right\rangle_{r\eta} \quad (1)$$

η is the coupling parameter that increased from 0 (reactant) to 1 (product). $\Delta_{\mathrm{dp}}E$ is the vertical energy gap, which is defined as the potential energy difference between the reactant and product states. This value is obtained from the FPMD trajectory produced by sampling the restrained mapping Hamiltonian:

$$H_\eta = (1-\eta)H_R + \eta H_P + V_r \quad (2)$$

Here H_R and H_P stand for the reactant and product states respectively. The harmonic restraint (V_r) is applied on the dummy atom to keep it in the location resembling the reactant state:

$$V_r = \sum_{bonds} \frac{1}{2}k_d (d-d_0)^2 + \sum_{angles} \frac{1}{2}k_\theta (\theta-\theta_0)^2 \quad (3)$$

This harmonic potential consists of the bond stretching and angle bending terms whose equilibrium values are d_0 and θ_0, respectively. The equilibrium values used for each surface group were derived from the simulations without restraints and the force constants k_d and k_θ were selected according to previous studies.[1, 3] The parameters of V_r are given in Table S2. The 3-point Simpson's rule (Eq. 4) was employed to evaluate

the integral in Eq. 1 for most of the surface groups. For ≡Fe_2OH on (010) surface and ≡Fe_2OH/≡Fe_2O_mH/≡Fe_3OH on (001) surface, the 5-point formula (Eq. 5) was used due to the significant nonlinearities of ΔE in these systems.

$$\Delta_{dp}A_{AH} = \frac{1}{6}\left(\langle \Delta E\rangle_0 + \langle \Delta E\rangle_1\right) + \frac{2}{3}\langle \Delta \mathrm{E}\rangle_{0.5} \quad (4)$$

$$\Delta_{dp}A_{AH} = \frac{1}{12}(\langle \Delta E\rangle_0 + \langle \Delta E\rangle_1 + 4(\langle \Delta E\rangle_{0.25} + \langle \Delta E\rangle_{0.75}) + 2\langle \Delta E\rangle_{0.5}) \quad (5)$$

With the same procedure, one proton of a hydronium located in the solution region is transformed into a dummy atom, and the associated free energy is calculated with Eq. 1. The final pK_a is calculated according to the formula:

$$2.3k_BTpK_a = \int_0^1 d\eta \left\langle \Delta_{dp}E_{AH} \right\rangle_{r\eta} - \int_0^1 d\eta \left\langle \Delta_{dp}E_{H_3O^+} \right\rangle_{r\eta} + k_BTln\left[c^0\Lambda^3_{H^+}\right] \quad (6)$$

c^0 = 1 mol/L is the unit molar concentration and $\Lambda^3_{H^+}$ means the thermal wavelength of the proton.[2] The last term stands for the translational entropy generated by the acid dissociation and can be approximated by the chemical potential of a free proton at the standard concentration, which equals -0.19 eV.

The convergence of the pK_a calculation was determined by monitoring the vertical energy gap. By taking ≡Fe_2OH and ≡Fe_2OH_2 on (010) surface as examples, Figure S2 shows the raw vertical energy gap data and the accumulative averages, where one can see that the vertical energy gaps were all converged within 0.05 eV in the periods. This is consistent with the observation in our previous calculations that ΔE converged on a typical FPMD timescale.[1, 4, 5]

Table S2. The parameters used for restraining the dummy atoms (harmonic potentials in Eq. (3)). H_d represents the dummy atom. n_d and n_θ mean the number of restrained

106 bonds and angles, respectively. d_0 stands for equilibrium bond lengths (in Bohr), and θ_0

107 stands for equilibrium angles (in radian).

Surface	Group	n_d	d_0	k_d	n_θ	θ_0	k_θ
(010)	≡Fe_2OH	1	1.89	1.0	2	2.02 (Fe-O-H_d)	0.1
						2.02 (Fe-O-H_d)	0.1
	≡Fe_2OH_2	2	1.89	1.0	3	2.00 (Fe-O-H_d)	0.1
			1.89	1.0		2.00 (Fe-O-H_d)	0.1
						1.80 (H-O-H_d)	0.1
	H_3O^+	3	1.89	1.0	2	1.94 (H-O-H_d)	0.1
			1.89	1.0		1.94 (H-O-H_d)	0.1
			1.89	1.0			
(001)	≡FeOH	1	1.89	1.0	1	1.94 (Fe-O-H_d)	0.1
	≡$FeOH_2$	2	1.89	1.0	2	2.24 (Fe-O-H_d)	0.1
			1.89	1.0		1.88 (H-O-H_d)	0.1
	≡Fe_2OH	1	1.89	1.0	2	1.95 (Fe-O-H_d)	0.1
						1.95 (Fe-O-H_d)	0.1
	≡Fe_2OH_2	2	1.89	1.0	3	1.88 (Fe-O-H_d)	0.1
			1.89	1.0		1.88 (Fe-O-H_d)	0.1
						1.81 (H-O-H_d)	0.1
	≡Fe_2O_mH	1	1.89	1.0	2	1.95 (Fe-O-H_d)	0.1
						1.95 (Fe-O-H_d)	0.1
	≡Fe_3OH	1	1.89	1.0	3	2.08 (Fe-O-H_d)	0.1

						2.08 (Fe-O-H_d)	0.1
						2.08 (Fe-O-H_d)	0.1
	H_3O^+	3	1.89	1.0	2	1.94 (H-O-H_d)	0.1
			1.89	1.0		1.94 (H-O-H_d)	0.1
			1.89	1.0			
(100)	≡FeO_UH_2	2	1.89	1.0	3	1.96 (Fe-O-H_d)	0.1
			1.89	1.0		1.82 (H-O-H_d)	0.1
						1.96 (Fe-O-H)	0.1
	≡FeO_LH_2	2	1.89	1.0	2	1.68 (Fe-O-H_d)	0.1
			1.89	1.0		1.80 (H-O-H_d)	0.1
	H_3O^+	3	1.89	1.0	2	1.94 (H-O-H_d)	0.1
			1.89	1.0		1.94 (H-O-H_d)	0.1
			1.89	1.0			

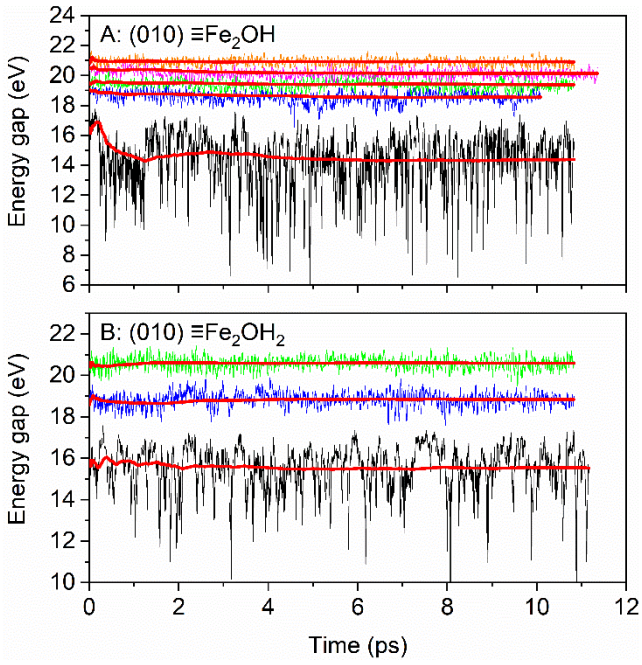

Figure S2. The accumulative averages of vertical energy gaps for (A) ≡Fe_2OH and (B) ≡Fe_2OH_2 on (010) surface. The statistical error was estimated as the difference between the first and the second half of the production run.

Table S3. Calculated vertical energy gaps (in eV), thermodynamic integrals (in eV), and pK_a values.

Surface	Group	η=0.0	η=0.25	η=0.5	η=0.75	η=1.0	ΔA	pK_a
(010)	$\equiv Fe_2OH$	14.38±0.02	18.56±0.04	19.39±0.02	20.14±0.03	20.91±0.02	19.07±0.03	11.5±0.7
	$\equiv Fe_2OH_2$	15.53±0.04		18.84±0.01		20.59±0.01	18.58±0.01	3.3±0.3
	H_3O^+	14.34±0.02		18.50±0.01		20.80±0.02	18.19±0.01	
(001)	$\equiv FeOH$	16.82±0.03		19.84±0.03		21.21±0.01	19.56±0.03	11.7±0.8
	$\equiv FeOH_2$	16.46±0.02		19.36±0.01		20.99±0.04	19.15±0.01	4.8±0.5
	$\equiv Fe_2OH$	15.95±0.03	18.70±0.05	19.35±0.02	20.17±0.01	20.73±0.01	19.24±0.03	6.3±0.8
	$\equiv Fe_2OH_2$	16.63±0.01		18.86±0.02		20.39±0.05	18.74±0.02	-2.0±0.7
	$\equiv Fe_2O_mH$	14.32±0.04	19.16±0.05	19.92±0.03	20.40±0.03	20.98±0.02	19.45±0.04	9.9±1.0
	$\equiv Fe_3OH$	16.09±0.01	18.55±0.04	19.21±0.04	19.98±0.05	20.70±0.02	19.11±0.04	4.2±1.0
	H_3O^+	15.06±0.05		19.04±0.01		20.81±0.04	18.67±0.02	
(100)	$\equiv FeO_UH_2$	14.03±0.04		19.01±0.02		20.73±0.05	18.47±0.03	6.0±0.8
	$\equiv FeO_LH_2$	14.98±0.02		19.77±0.03		21.21±0.02	19.21±0.02	18.4±0.7

H_3O^+	14.42±0.04	18.10±0.01	20.71±0.05	17.92±0.02

S3. Free energy calculation

The desorption free energies of As(V) from lepidocrocite and goethite surfaces were evaluated according to the thermodynamic integration relation:[6]

$$\Delta F(X) = -\int_{X0}^{X} f(X')\,\mathrm{d}X' \tag{7}$$

where ΔF stands for the free energy change, X means the reaction coordinate, and f is the mean force. The mean forces were derived by using the method of constraint in the blue-moon ensemble. Figure 2 and Figure S3 present the initial configurations of As(V) species on lepidocrocite (001) and goethite (110) surfaces, respectively. As(V) species were placed on only one side of the surface slab, which was the common practice in the simulation community. On both surfaces, As(V) species were separated from their periodic images by about four layers of water, which was enough to minimize the adsorbate-adsorbate interactions. The surface coverages were estimated to be ~0.21 mg/m^2 (~1.46 μmol/m^2) for lepidocrocite (001) surface and ~0.24 mg/m^2 (~1.66 μmol/m^2) for goethite (110) surface. These values are similar to 1.40 μmol/m^2 reported in Mamindy-Pajany et al. [7].

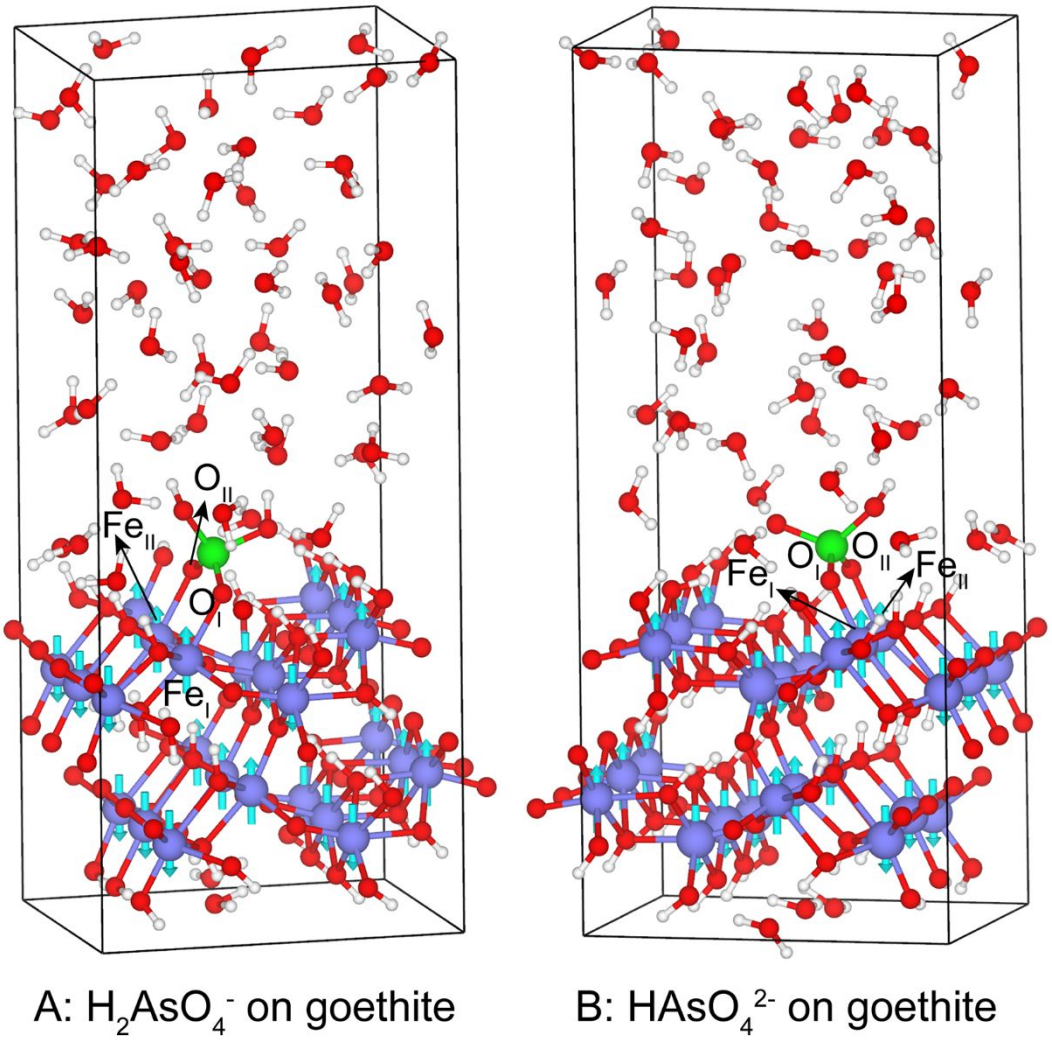

Figure S3. Models used for (A) $H_2AsO_4^-$ and (B) $HAsO_4^{2-}$ complexation on goethite (110) surface. oxygen = red, hydrogen = white, iron = blue-violet, arsenic = green. Cyan arrows indicate the electron spin orientations.

S4. FPMD details

All FPMD simulations were performed using CP2K/QUICKSTEP package.[8-10] The electronic structures were calculated with the Gaussian and Plane Wave (GPW) density functional scheme.[11] The electronic wavefunctions were constructed using a double-ζ Gaussian-type orbital basis with polarization functions (DZVP) and the electron density was represented with the plane-wave basis expanded to 360 Ry. The core electron states

were described using Goedecker-Teter-Hutter (GTH) pseudopotentials.[12] The exchange-correlation interaction was treated in the generalized gradient approximation (GGA) in the parameterization of Perdew, Burke, and Ernzerhof (PBE).[13] The GGA+U approach with a U_{eff} correction value of 4 eV was adopted to correct the description of 3d electrons in Fe atoms in lepidocrocite.[14] Van der Waals corrections were included with the DFT-D3 method.[15] Wave functions were optimized to a tolerance of 1.0E-6.

Antiferromagnetic ordering was adopted for goethite and lepidocrocite following previous simulations.[16-21] The antiferromagnetic spin structure determined by Guo and Barnard [22] was applied for lepidocrocite, where Fe atoms in the same double-layer had antiparallel spins (Figure 1). For goethite, antiparallel spins on alternating layers along [010] direction were adopted (Figure S3).[21] The predicted band gap for lepidocrocite was 1.85 eV, close to the experimental value 2.06 eV. [23] The total magnetic moments of lepidocrocite and goethite were calculated to be zero, in agreement with their antiferromagnetic properties.

Born-Oppenheimer type molecular dynamics (BOMD) simulations were carried out in NVT ensemble with a time step of 0.5 fs. The temperature was maintained at 330 K with the Nosé-Hoover chain thermostat to avoid the glassy behavior of DFT liquid water at a lower temperature.[24] For each FPMD simulation, a production run was performed for over 10.0 ps after an equilibration run for at least 5.0 ps.

S5. Interfacial structures

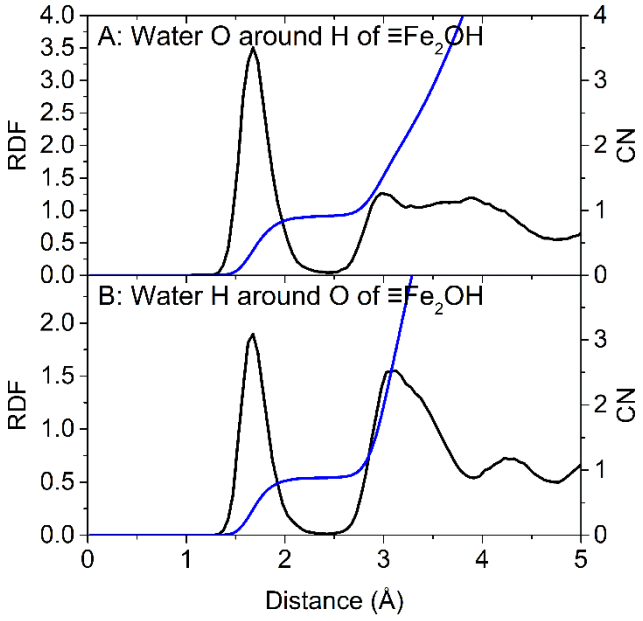

Figure S4. Radial distribution function (RDF) and coordination number (CN) for (A) water O around H of ≡Fe_2OH and (B) water H around O of ≡Fe_2OH on (010) surface.

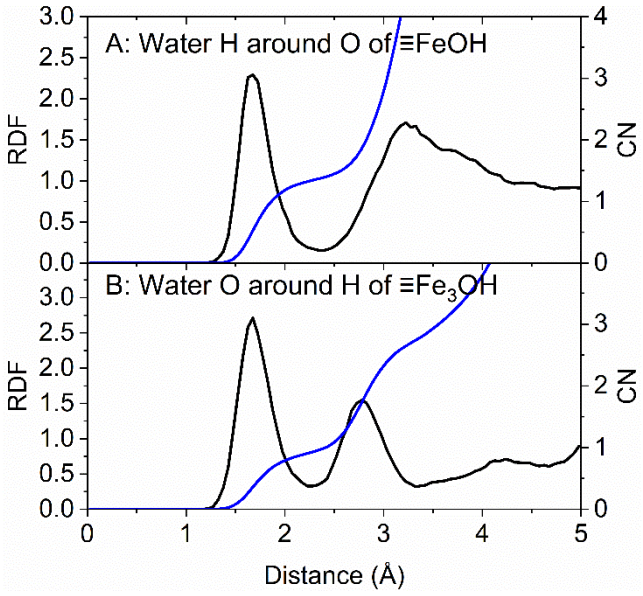

Figure S5. RDF and CN for (A) water H around O of ≡FeOH and (B) water O around H of ≡Fe_3OH on (001) surface.

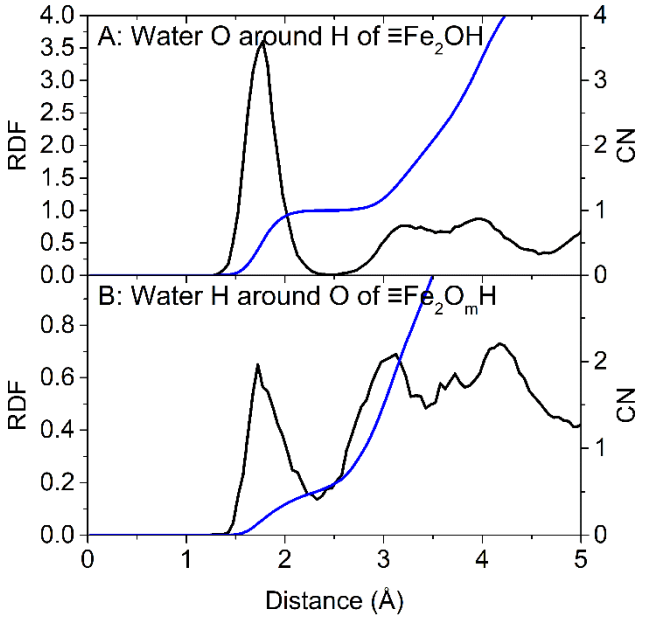

Figure S6. RDF and CN for (A) water O around H of ≡Fe_2OH and (B) water H around O of ≡Fe_2O_mH on (001) surface.

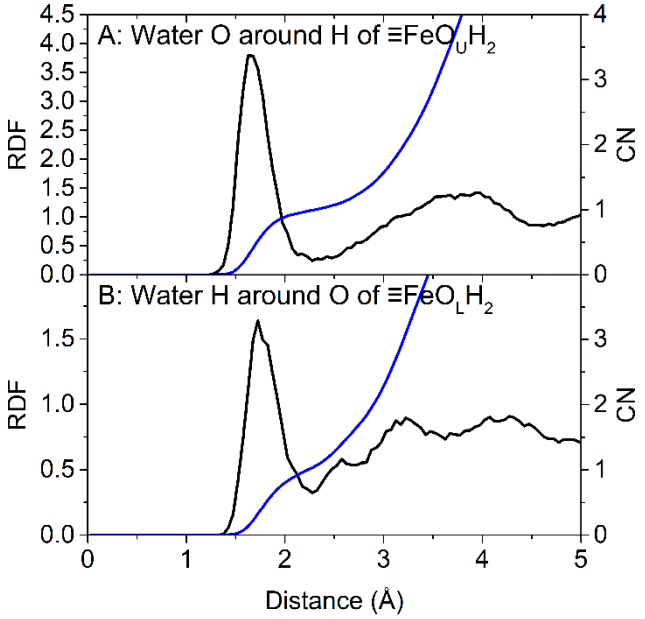

Figure S7. RDF and CN for (A) water O around H of ≡FeO_UH_2 and (B) water H around O of ≡FeO_LH_2 on (100) surface.

S6. Additional information for the desorption processes

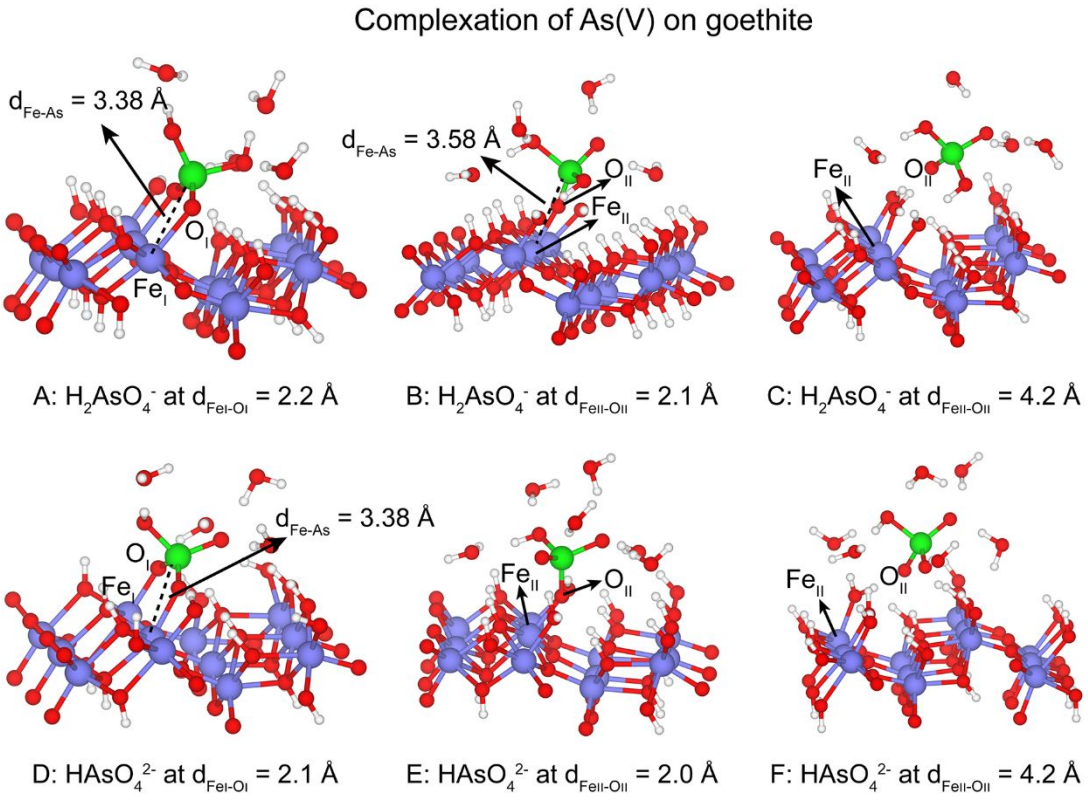

175

176 Figure S8. Snapshots of As(V) complexes on goethite (110) surface. Atoms are color-

177 coded by element as described in Figure S3. Only the water molecules that hydrogen-

178 bonded with As(V) species are depicted for clarity.

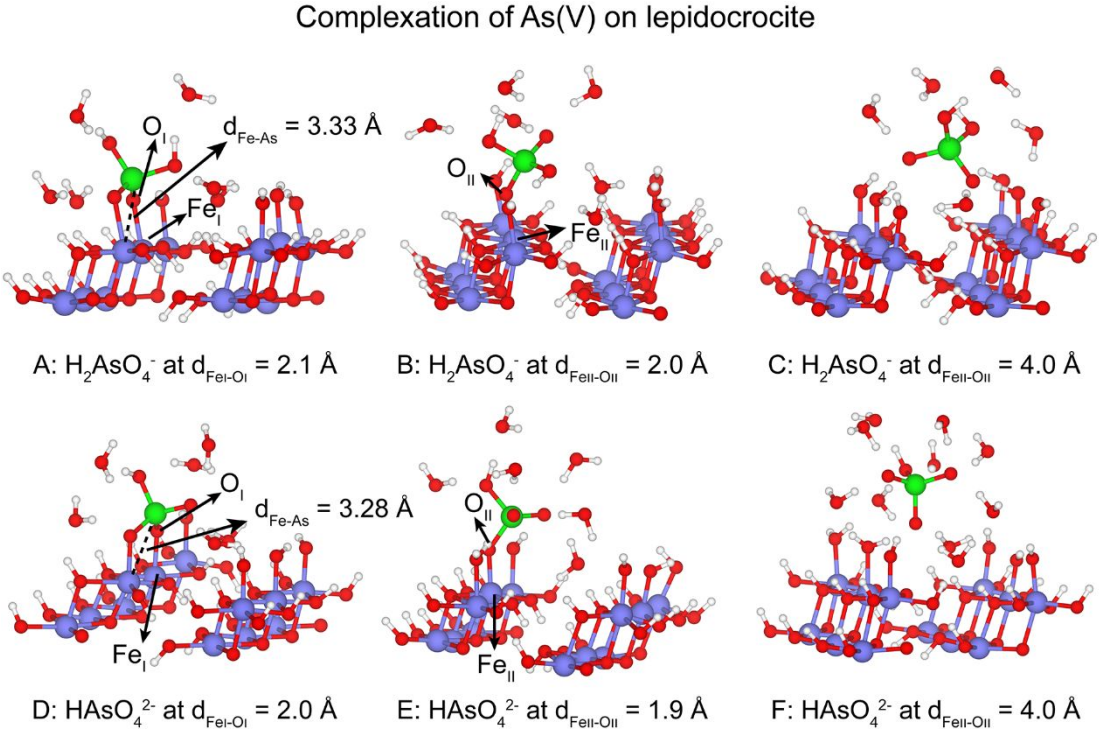

179

Figure S9. Snapshots of As(V) complexes on lepidocrocite (001) surface. Atoms are color-coded by element as described in Figure S3. Only the water molecules that hydrogen-bonded with As(V) species are depicted for clarity.

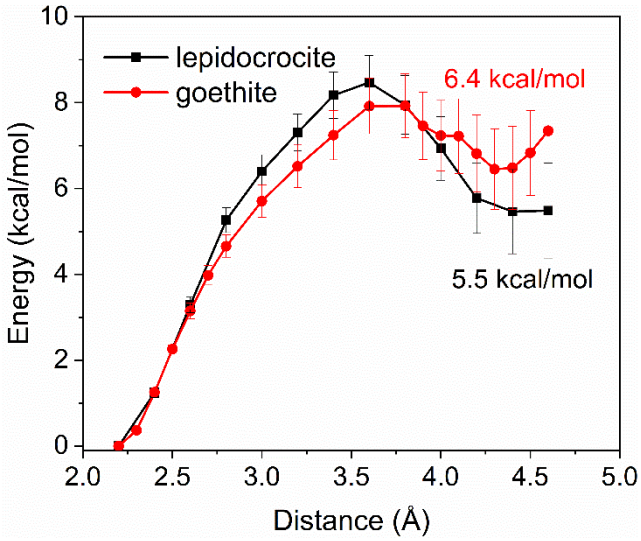

Figure S10. Desorption free energy curves of coordinated water on goethite (110) and lepidocrocite (001) surfaces.

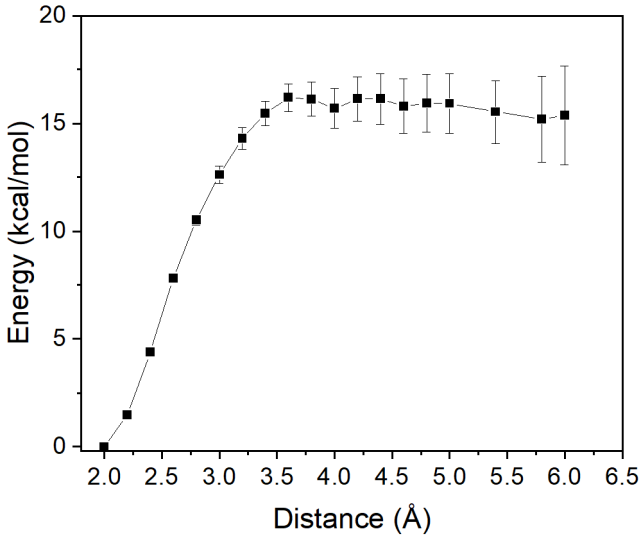

Figure S11. The extended desorption free energy curve of $H_2AsO_4^-$ on lepidocrocite (001) surface.

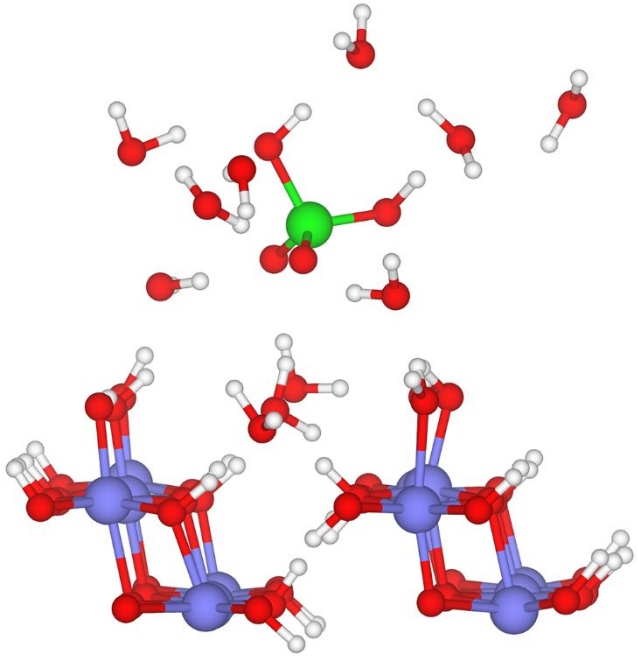

Figure S12. Snapshot of $H_2AsO_4^-$ on lepidocrocite (001) surface at Fe_{II}-O_{II} distance of 6.0 Å. Atoms are color-coded by element as described in Figure S3. Only the water molecules that hydrogen-bonded with $H_2AsO_4^-$ are depicted for clarity.

Table S4. The average Fe-As distances of As(V) complexes on goethite and lepidocrocite.

Iron oxyhydroxides	Surface	Complexes	Fe-As distance (Å)
Lepidocrocite	(001)	$H_2AsO_4^-$ bidentate	3.33
	(100)	$HAsO_4^{2-}$ bidentate	3.33
		$H_2AsO_4^-$ bidentate	3.33
Goethite	(110)	$HAsO_4^{2-}$ bidentate	3.38
		$H_2AsO_4^-$ bidentate	3.38
		$H_2AsO_4^-$ monodentate	3.58
	(010)	$HAsO_4^{2-}$ bidentate	3.41
		$H_2AsO_4^-$ bidentate	3.43

(021)	$H_2AsO_4^-$ monodentate	3.68	

Table S5. The simulation types and net charges of systems presented in Figure 6.

Iron hydroxides	surface	As(V) species	Simulation type	Free energy calculation?	Net charge
Goethite	(110)	$HAsO_4^{2-}$	Constrained FPMD	Yes	0
		$H_2AsO_4^-$	Constrained FPMD	Yes	+1
	(010)	$HAsO_4^{2-}$	FPMD	No	-2
		$H_2AsO_4^-$	FPMD	No	-1
	(021)	$H_2AsO_4^-$	FPMD	No	-1
Lepidocrocite	(001)	$HAsO4^{2-}$	Constrained FPMD	Yes	0
		$H_2AsO_4^-$	Constrained FPMD	Yes	+1
	(100)	$HAsO_4^{2-}$	FPMD	No	-2
		$H_2AsO_4^-$	FPMD	No	-1

REFERENCES

(1) Cheng, J.; Sulpizi, M.; Sprik, M., Redox potentials and pKa for benzoquinone from density functional theory based molecular dynamics. *J. Chem. Phys.* **2009,** *131*, (15), 154504.

(2) Costanzo, F.; Sulpizi, M.; Valle, R. G. D.; Sprik, M., The oxidation of tyrosine and tryptophan studied by a molecular dynamics normal hydrogen electrode. *J. Chem. Phys.* **2011,** *134*, (24), 244508.

(3) Sulpizi, M.; Sprik, M., Acidity constants from vertical energy gaps: density functional theory based molecular dynamics implementation. *Phys. Chem. Chem. Phys.* **2008,** *10*, (34), 5238-5249.

(4) Liu, X.; Lu, X.; Sprik, M.; Cheng, J.; Meijer, E. J.; Wang, R., Acidity of edge surface sites of montmorillonite and kaolinite. *Geochim. Cosmochim. Acta* **2013,** *117*, 180-190.

(5) Cheng, J.; Liu, X.; VandeVondele, J.; Sulpizi, M.; Sprik, M., Redox Potentials and Acidity Constants from Density Functional Theory Based Molecular Dynamics. *Acc. Chem. Res.* **2014,** *47*, (12), 3522-3529.

(6) Sprik, M.; Ciccotti, G., Free energy from constrained molecular dynamics. *J. Chem. Phys.* **1998,** *109*, (18), 7737-7744.

(7) Mamindy-Pajany, Y.; Hurel, C.; Marmier, N.; Roméo, M., Arsenic (V) adsorption from aqueous solution onto goethite, hematite, magnetite and zero-valent iron: Effects of pH, concentration and reversibility. *Desalination* **2011,** *281*, 93-99.

(8) VandeVondele, J.; Krack, M.; Mohamed, F.; Parrinello, M.; Chassaing, T.; Hutter, J., Quickstep: Fast and accurate density functional calculations using a mixed Gaussian and plane waves approach. *Comput. Phys. Commun.* **2005,** *167*, (2), 103-128.

(9) Hutter, J.; Iannuzzi, M.; Schiffmann, F.; VandeVondele, J., CP2K: atomistic simulations of condensed matter systems. *Wires. Comput. Mol. Sci.* **2014,** *4*, (1), 15-25.

(10) Kühne, T. D.; Iannuzzi, M.; Del Ben, M.; Rybkin, V. V.; Seewald, P.; Stein, F.; Laino, T.; Khaliullin, R. Z.; Schütt, O.; Schiffmann, F.; Golze, D.; Wilhelm, J.; Chulkov, S.; Bani-Hashemian, M. H.; Weber, V.; Borštnik, U.; Taillefumier, M.; Jakobovits, A. S.; Lazzaro, A.; Pabst, H.; Müller, T.; Schade, R.; Guidon, M.; Andermatt, S.; Holmberg, N.; Schenter, G. K.; Hehn, A.; Bussy, A.; Belleflamme, F.; Tabacchi, G.; Glöß, A.; Lass, M.; Bethune, I.; Mundy, C. J.; Plessl, C.; Watkins, M.; VandeVondele, J.; Krack, M.; Hutter, J., CP2K: An electronic structure and molecular dynamics software package - Quickstep: Efficient and accurate electronic structure calculations. *J. Chem. Phys.* **2020,** *152*, (19), 194103.

(11) Lippert, B. G.; Hutter, J.; Parrinello, M., A hybrid Gaussian and plane wave density functional scheme. *Mol. Phys.* **1997,** *92*, (92), 477-487.

(12) Goedecker, S.; Teter, M.; Hutter, J., Separable dual-space Gaussian pseudopotentials. *Phys. Rev. B* **1995,** *54*, (3), 1703--1710.

(13) Perdew, J. P.; Burke, K.; Ernzerhof, M., Generalized Gradient Approximation Made Simple. *Phys. Rev. Lett.* **1997,** *78*, (7), 1396.

(14) Pope, D. J.; Clark, A. E.; Rosso, K. M.; Prange, M. P., Rethinking the magnetic properties of lepidocrocite: A density functional theory and cluster expansion study. *J. Appl. Phys.* **2020,** *128*, (10), 103906.

(15) Grimme, S.; Antony, J.; Ehrlich, S.; Krieg, H., A consistent and accurate ab initio parametrization of density functional dispersion correction (DFT-D) for the 94 elements H-Pu. *J. Chem. Phys.* **2010,** *132*, (15), 154104.
(16) Borowski, S. C.; Biswakarma, J.; Kang, K.; Schenkeveld, W. D. C.; Hering, J. G.; Kubicki, J. D.; Kraemer, S. M.; Hug, S. J., Structure and reactivity of oxalate surface complexes on lepidocrocite derived from infrared spectroscopy, DFT-calculations, adsorption, dissolution and photochemical experiments. *Geochim. Cosmochim. Acta* **2018,** *226*, 244-262.
(17) Guo, H.; Barnard, A. S., Proton transfer in the hydrogen-bonded chains of lepidocrocite: a computational study. *Phys. Chem. Chem. Phys.* **2011,** *13*, (39), 17864-17869.
(18) Davantès, A.; Costa, D.; Lefèvre, G., Molybdenum(VI) Adsorption onto Lepidocrocite (γ-FeOOH): In Situ Vibrational Spectroscopy and DFT+U Theoretical Study. *J. Phys. Chem. C* **2016,** *120*, (22), 11871-11881.
(19) McBriarty, M. E.; Soltis, J. A.; Kerisit, S.; Qafoku, O.; Bowden, M. E.; Bylaska, E. J.; De Yoreo, J. J.; Ilton, E. S., Trace Uranium Partitioning in a Multiphase Nano-FeOOH System. *Environ. Sci. Technol.* **2017,** *51*, (9), 4970-4977.
(20) Tunega, D.; Zaoui, A., Adsorption of polycyclic aromatic hydrocarbons on FeOOH polymorphs: A theoretical study. *Surf. Sci.* **2021,** *706*, 121795.
(21) Zhang, Y.; Liu, X.; Cheng, J.; Lu, X., Interfacial structures and acidity constants of goethite from first principles molecular dynamics simulation. *Am. Mineral.* **2021,** *106*, (11), 1736-1743.
(22) Guo, H.; Barnard, A. S., Modeling the iron oxides and oxyhydroxides for the prediction of environmentally sensitive phase transformations. *Phys. Rev. B* **2011,** *83*, (9), 094112.
(23) Cornell, R. M.; Schwertmann, U., *The iron oxides: structure, properties, reactions, occurrences and uses*. John Wiley & Sons: 2003.
(24) VandeVondele, J.; Mohamed, F.; Krack, M.; Hutter, J.; Sprik, M.; Parrinello, M., The influence of temperature and density functional models in ab initio molecular dynamics simulation of liquid water. *J. Chem. Phys.* **2005,** *122*, (1), 014515.